Journal of Power Sources 264 (2014) 282–289

Contents lists available at ScienceDirect

Journal of Power Sources

journal homepage: www.elsevier.com/locate/jpowsour

# Ni–WC/C nanocluster catalysts for urea electrooxidation

Lu Wang, Mingtao Li, Zhiyu Huang, Yingming Li, Suitao Qi, Chunhai Yi, Bolun Yang*

*Department of Chemical Engineering, State Key Laboratory of Multiphase Flow in Power Engineering, Xi'an Jiaotong University, Xi'an, 710049, PR China*

## HIGHLIGHTS

- The Ni–WC/C catalysts were prepared successfully by a simple impregnation method.
- The nickel particles were grown on the WC/C framework in clusters with nanoscale.
- Tungsten carbide promotes nickel to more active sites for urea electrooxidation.
- Ni–WC/C nanoclusters show superior catalytic activity for urea electrooxidation.

## GRAPHICAL ABSTRACT

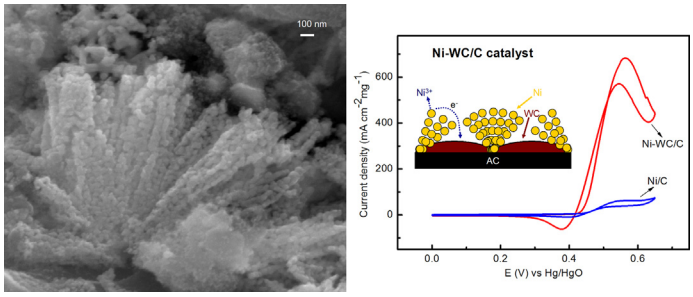


## ARTICLE INFO

*Article history:*
Received 21 November 2013
Received in revised form
25 March 2014
Accepted 21 April 2014
Available online 30 April 2014

*Keywords:*
Nanostructure electrocatalysts
Tungsten carbide
Synergistic effect
Electrooxidation of urea

## ABSTRACT

A nanocluster Ni–WC/C electrocatalyst is prepared through a sequential impregnation method and is used for the urea electrooxidation in alkaline conditions. The micro-morphology, lattice parameter, composition and surface states of Ni–WC/C particles are determined by scanning electron microscopy (SEM), transmission electron microscopy (TEM), X-ray diffraction (XRD), energy dispersive X-ray (EDX) and X-ray photoelectron spectrometry (XPS) analysis. The electrooxidation activity and stability of the Ni–WC/C catalyst are also investigated by cyclic voltammograms and chronoamperograms. Characterization results indicate that the Ni nanoclusters are uniformly distributed on the WC/C framework, and the Ni–WC/C catalyst shows high electrocatalytic activity and stability for urea electrooxidation. The maximum current density at the Ni–WC/C electrode is almost 700 mA $cm^{-2}$ $mg^{-1}$ which is one order of magnitude higher than that at the Ni/C electrode, and the steady current density at the Ni–WC/C electrode is also markedly improved. Furthermore, the ESA values and XPS spectra indicate that the enhanced performance of the Ni–WC/C catalyst could be attributed to the structure effect and electron effect between nickel and tungsten carbide.



## 1. Introduction

To deal with the problem of energy shortage and to protect the global environment, hydrogen has been identified as one of the most promising candidates for alternative energy sources. Urea ($CO(NH_2)_2$) has been considered as a hydrogen carrier for long-term sustainable energy supply due to its stable, relatively non-toxic, non-flammable and renewable properties [1,2]. In addition, urea-rich wastewater is produced in abundance from both animal excreta and industrial synthesis of urea [3–5]. Recently, the electrochemical treatment for urea-rich wastewater simultaneously generating hydrogen has attracted considerable attention [3,5–8] since it is an efficient, clean and well-controlled technique. Furthermore, the urea electrooxidation process is also economical because it avoids the use of noble-metal catalysts which are

* Corresponding author. Tel.: +86 29 82663189; fax: +86 29 82668789.
*E-mail address:* blunyang@mail.xjtu.edu.cn (B. Yang).

http://dx.doi.org/10.1016/j.jpowsour.2014.04.104
0378-7753/

expensive and scarce. In alkaline media, the low cost nickel electrode is shown to be an effective catalyst for urea electrooxidation [9,10]. The reaction process associated with the urea electrooxidation can be summarized as follows.

$$Ni + 2OH^- \rightarrow Ni(OH)_2 + 2e^- \quad (1)$$

$$Ni(OH)_2 + OH \rightarrow NiOOH + H_2O + e^- \quad (2)$$

$$CO(NH_2)_2 + 6NiOOH + H_2O \rightarrow 6Ni(OH)_2 + N_2 + CO_2 \quad (3)$$

Net anode reaction:

$$CO(NH_2)_2 + 6OH^- \rightarrow N_2 + 5H_2O + CO_2 + 6e^- \quad (4)$$

The nickel is firstly oxidized to $Ni(OH)_2$ in the alkaline solution (Eq. (1)); then the $Ni(OH)_2$ undergoes oxidation to its active NiOOH form at high potential, as per Eq. (2); the NiOOH oxidizes urea further to regenerate the $Ni(OH)_2$, shown in Eq. (3). During the electrochemical oxidation of urea in an alkaline media, NiOOH catalyzes urea electrooxidation to the products at the anode, and the net anode reaction is depicted as Eq (4). [3,11,12] From the total urea electrooxidation reaction, it can be observed that the NiOOH acts as the catalytic active form, however, the active nickel oxide state (NiOOH) would be generated at high potential, and it could be easily blocked by CO groups as urea is oxidized which leads to the deactivation of catalysts. [8,12] As a result, the current density indicating reaction kinetics of Eq. (3) is low because of the unavailability of NiOOH, and it quickly decreases due to a deactivated catalytic surface. Thus, to obtain a high and steady current density, more active form (NiOOH) should be produced and simultaneously the CO blockage of NiOOH should also be minimized.

Several methods of enhancement have been developed to increase active sites and restrain the CO blockage for urea electrooxidation to reach a high current density. One way is to synthesize the nanostructure catalysts by taking advantages of their excellent electrical properties [13] and large surface area to enhance the current density. A series of catalysts with nanostructure, such as nanosheets [14], nanoribbons [13] and nanotubes nickel hydroxide [1], have been successfully prepared and investigated for urea electrooxidation. The obtained maximum current densities were 154, 5 and 50 mA $cm^{-2}$ $mg^{-1}$, respectively, which were much higher than that at the bulk nickel hydroxide electrode (0.5 mA $cm^{-2}$ $mg^{-1}$). However, these nanostructure nickel hydroxides cannot effectively overcome CO poisoning, the current densities thus would decrease quickly due to the catalyst deactivation. To improve the CO-tolerance of catalysts, Botte et al. synthesized bimetallic and polymetallic electrocatalysts by electroplating other noble metals on nickel foil, such as Pt–Ni, Pt–Ir–Ni, Rh–Ni and Ru–Ni [8]. Among these, the electrodeposited Rh on Ni foil offers the best performance, which can yield a steady current density to 50 mA $cm^{-2}$, improving by a factor of 200 compared to a Ni catalyst [3]. This is probably due to the ability of the rhodium in the Rh–Ni electrode to selectively adsorb CO, thus preventing nickel from CO poisoning and leaving active sites for the adsorption of the urea molecule [8]. However, the CO adsorption on Rh is still somewhat limited [7], and additionally the increased amount of precious metal usage results in high cost [15]. Therefore, more efficient catalysts need to be explored urgently in order to achieve a high current density and maintain activity for a long time.

Recently, tungsten carbide (WC) has been used as a high efficient co-catalyst to enhance the activity and stability for several electrochemical reactions [16–18]. Furthermore, tungsten carbide is known to be highly resistant to CO poisoning and stable in acidic and basic solutions [19–21], which could also significantly increase the stability of catalysts [22]. Ganesan et al. found that Pt supported on WC exhibited high methanol oxidation reaction (MOR) activity [23,24]. The high activity could be attributed to the fact that WC activates methanol to form a methoxy intermediate, and further decomposition of the methoxy species is promoted by Pt [22]. In addition, Lee et al. reported that Pt/WC exhibited much improved resistance to CO poisoning compared to a Pt/C catalyst [25]. The results can be explained by the weak surface adsorption of CO on WC so that temporary blockage on the active catalytic sites is relieved. [26] On the other hand, tungsten carbide also has other unique physical and chemical characteristics, such as high hardness, temperature stability, excellent electrical conductivity, and especially, lower cost [27,28].

In particular, WC is shown to have a broad unoccupied d band (or more likely, hybrid tungsten 5d, carbon 2p bands) above $E_F$-broader, in fact, broader than the unoccupied d band of tungsten [29,30]. This characteristic allows tungsten carbide to attract the outer-layer electron of Ni atom, which would tend to make nickel lose electron, allowing it to reach its active oxide state (NiOOH) for urea electrooxidation. Furthermore, as NiOOH is easily blocked by CO groups, a weak surface adsorption of CO on WC would enhance the CO-tolerance of the catalyst. Therefore, tungsten carbide may be used as a co-catalyst working together with nickel to enhance the activity and CO-tolerance in the urea electrooxidation process.

In the present study, the nanostructure Ni-based electrocatalyst with tungsten carbide was prepared by a sequential impregnation method for catalytic urea electrooxidation. Considering that the low specific surface area of WC is unfavorable for the dispersion of nickel particles [17,20,31], activated carbon was utilized as carrier which can contribute to the generation of nanosized nickel with more active sites [32–34].

## 2. Experimental

### 2.1. Preparation of nanocluster Ni–WC/C catalysts

The fabrication procedure is illustrated schematically in Fig. 1. First, 2 g of activated carbon (Aladdin, 1000 $m^2$ $g^{-1}$) was impregnated in an ammonium paratungstate (AMT, from Aldrich, 99%) aqueous solution for the temperature-programming reduction (TPR) treatment. The sample was heated from 293 K to 923 K at a rate of 210 K $h^{-1}$ in a stream of 80 ml $min^{-1}$ $N_2$, followed by the reduction and carburization processes in a mixture of $H_2$ (80 ml $min^{-1}$)–$CH_4$ (20 ml $min^{-1}$) from 923 K to 1223 K at a ramping rate of 100 K $h^{-1}$, finishing at 1223 K for 2 h. The as-obtained solid is denoted as WC/C.

The as-prepared WC/C powder was added to a $Ni(NO_3)_2$ aqueous solution by incipient wetness impregnation. The TPR treatment

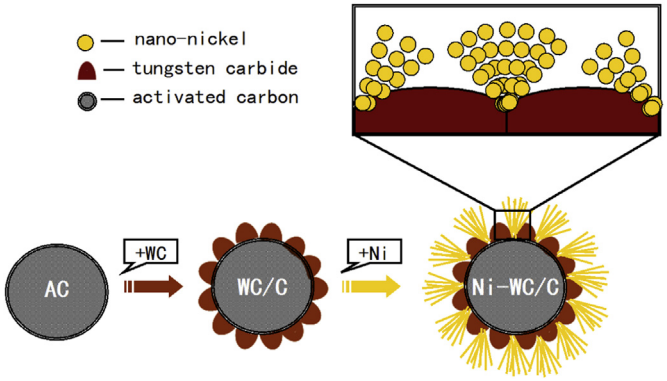


**Fig. 1.** Scheme of the fabrication procedure of the Ni–WC/C catalyst.

was carried out from 293 K to 723 K at a ramping rate of 430 K $h^{-1}$ in a steam of 60 ml $min^{-1}$ $N_2$ and 40 ml $min^{-1}$ $H_2$, finishing at 723 K for 2 h. These processes resulted in nano-Ni particles loaded on WC/C (noted as Ni–WC/C). Thus, different contents of the Ni–WC/C catalysts (see Table 1) were prepared to find an optimum composition for urea electrooxidation. As control, Ni particles were supported on the activated carbon by the same procedures, noted as Ni/C.

### 2.2. Electrochemical measurements

For anodic catalyst selection, the glassy carbon disk electrode (GCE, from CH Instruments) was polished and modified for working electrode. Details of the GCE pretreatment process are as follows.

1) A glassy carbon disk electrode, 3 mm in diameter, was polished with 0.05 μm alumina until the surface became mirror-like for working substrate before each experiment.
2) 3 mg of the prepared catalyst power was ultrasonicated in 0.5 ml of isopropanol, 2 ml of deionized water and 50 μl of 5 wt% Nafion solution for 5 min to get a suspension [35].
3) 5 μl of the suspension was dropped onto the polished GCE and dried at room temperature overnight.
4) After drying, the modified electrode was activated by 50 cycles of cyclic voltammetries from 0 to 0.65 V vs. Hg/HgO at 20 mV $s^{-1}$ in 1 M KOH and then used as the working electrode in all electrochemical measurements.

The control experiments used the Ni/C powder with the Nafion binder modified GCE as the working electrode which was pretreated as described above. All electrochemical measurements were performed in 1 M KOH in the absence and presence of 0.33 M urea aqueous solution using a CHI760D instrument. Nitrogen gas was bubbled into the solution for 30 min before the tests. An Hg/HgO electrode and platinum wire were chosen as the reference and counter electrodes, respectively. The cyclic voltammograms (CVs) were obtained between 0 and 0.65 V vs. Hg/HgO at a scan rate of 10 mV $s^{-1}$. All the voltammograms reported were from the sustained periodic state achieved after 20 sweeps. The chronoamperograms were carried out at a constant potential of 0.50 V vs. Hg/HgO for 1 h.

### 2.3. Materials characterization

The morphological characteristics of the synthesized catalysts were analyzed by field emission scanning electron microscopy (FESEM), using a FEI Quanta 600 FEG system operated at 20 kV. The chemical compositions of the prepared Ni–WC/C catalysts were determined by energy dispersive X-ray (EDX) attached to the FESEM. Transmission electron microscopy (TEM) images were performed on a Hitachi JEM-2100F at 200 kV. The crystalline structures were determined on an X-ray diffraction (XRD), using Rigaku D/max-2400 with a Cu Ka radiation. The surface states of the samples were characterized by X-ray photoemission spectroscopy (XPS, K-Alpha).

**Table 1**
Experimental matrix for the synthesis of different contents of Ni–WC/C (samples A–E) catalysts (wt.%).

| Catalysts | Nominal content | | | Determined by EDX | | |
|---|---|---|---|---|---|---|
| | Ni | WC | C | Ni | W | C |
| Sample A | 10 | 10 | 80 | 13.41 | 7.38 | 79.21 |
| Sample B | 10 | 20 | 70 | 10.36 | 11.09 | 78.55 |
| Sample C | 20 | 10 | 70 | 16.58 | 4.22 | 79.20 |
| Sample D | 20 | 20 | 60 | 21.12 | 11.06 | 67.82 |
| Sample E | 30 | 10 | 60 | 45.64 | 9.79 | 44.57 |

## 3. Results and discussion

### 3.1. Characterizations of nanocluster Ni–WC/C catalysts

The typical X-ray diffraction (XRD) patterns of the resulting Ni–WC/C particles (samples A–E) are presented in Fig. 2. Three characteristic peaks of each spectrum for nickel ($2\theta = 44.5°$, 51.8°, and 76.4°), corresponding to Miller indices (111), (200), and (222) [36], are observed. This reveals that the resultant particles consist of the face-centered cubic (fcc) nickel, which agrees well with the high-resolution TEM image (see Fig. 4b). Also, XRD analysis shows the existence of nanocrystalline tungsten carbide. The peaks at the $2\theta$ of 31.54, 35.66 and 48.44 with the $d$ values of 0.2834, 0.2516 and 0.1878 nm correspond to the (001), (100) and (101) facets of WC [37], which can also be observed from the high-resolution TEM image (see Fig. 4b). No peaks corresponding to W or $WO_x$ are detected, verifying the relative purity phase of the tungsten carbides in the prepared catalysts. The results in Fig. 2 indicate the coexistence of crystalline Ni and WC of the prepared catalyst, which are consistent with the EDX data (Little $W_2C$ is typically detected due to the calcining process). Furthermore, it can be seen that different contents of Ni–WC/C (samples A–E) share the same crystal structure from XRD, confirming a good reproducibility of the catalysts by this preparation method. Accordingly, it can be concluded that the nanoparticles prepared in this work include nickel of face-centered cubic (fcc) structure and tungsten carbide of hexagonal-close packed (hcp) structure as major phases.

The morphology images of the Ni–WC/C nanocluster catalyst are shown in Fig. 3a. For a further comparison of the morphology before and after the Ni loaded, the SEM images of WC/C and Ni–WC/C at the same magnification are shown in Fig. 3b and c, respectively. From Fig. 3a, a homogeneous distribution of small, uniform rounded grains can be seen; in addition, a flower growth and nanocluster structure can been found from the higher magnification SEM image (the inset of Fig. 3a). From Fig. 3b, we can see that the WC particles are uniformly dispersed on the activated carbon, which is corroborated by the EDX (the inset of Fig. 3b). And then the nanoscale rounded grains which have been found to be nickel (the inset EDX of Fig. 3c) are in clusters on the WC/C framework. Contrasting with the images of Fig. 3b and c, it can be

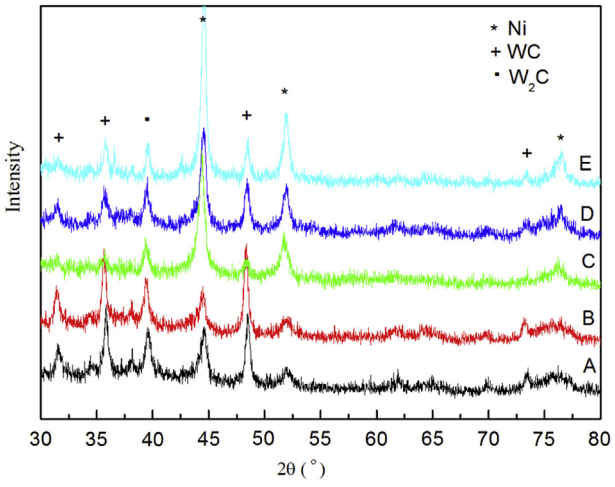


**Fig. 2.** XRD patterns of samples A–E particles. (A) 10% Ni–10% WC/C, (B) 10% Ni–20% WC/C, (C) 20% Ni–10% WC/C, (D) 20% Ni–20% WC/C, (E) 30% Ni–10% WC/C.

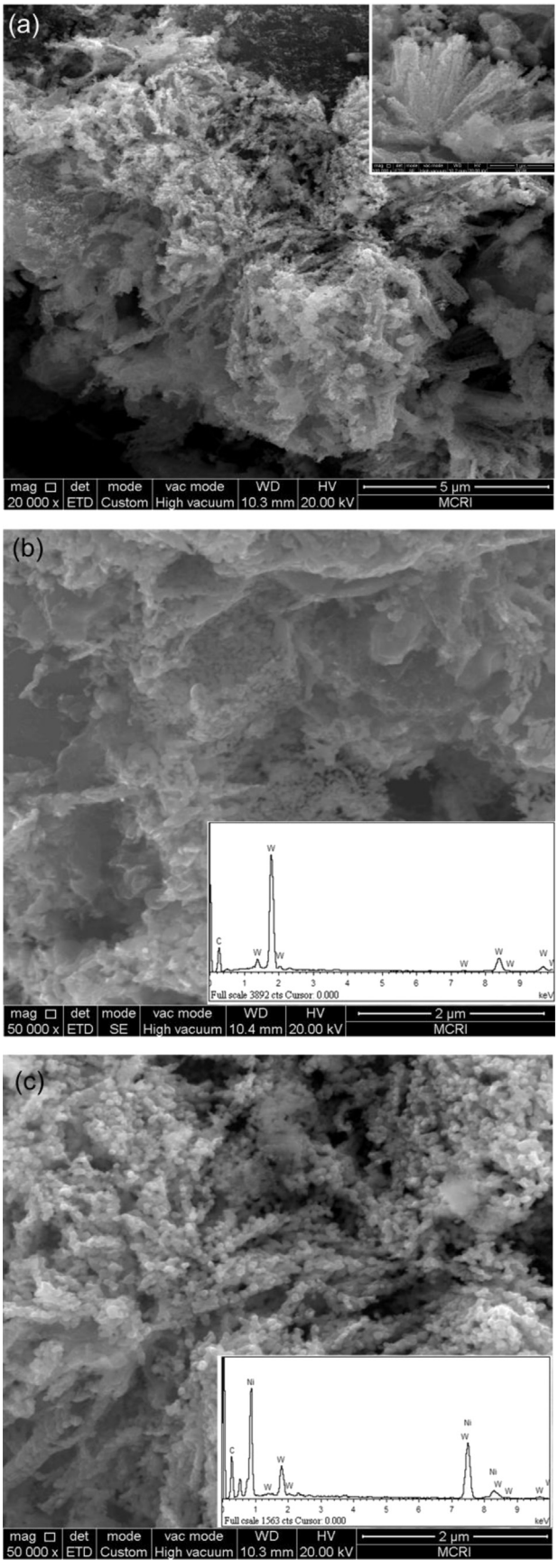


**Fig. 3.** (a) SEM images of the 20% Ni–20% WC/C catalyst. The inset is a high magnification image of this catalyst. (b), (c) SEM images with the same magnification of 20% WC/C and 20% Ni–20% WC/C catalysts, respectively.

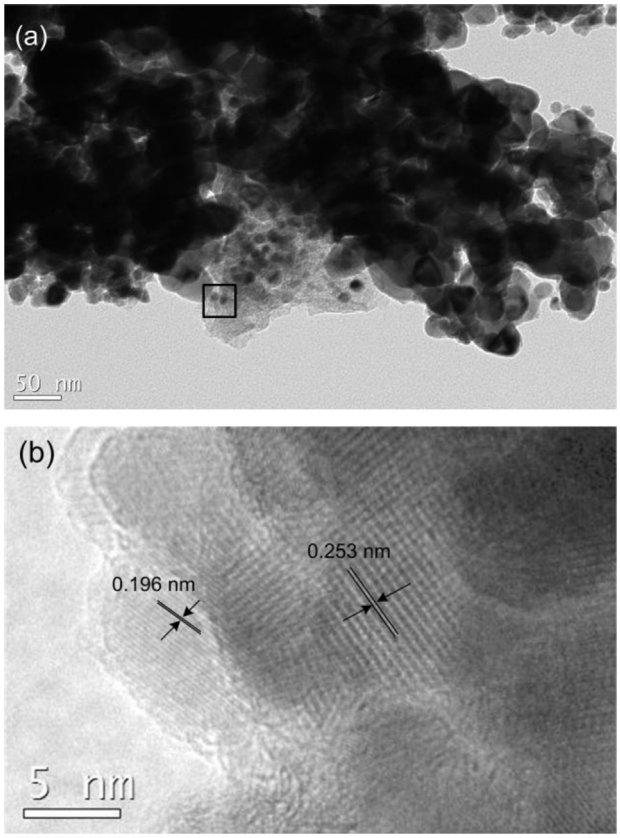


**Fig. 4.** (a) The TEM image of the 20% Ni–20% WC/C catalyst, (b) The high-resolution TEM image from the marked area.

clearly seen that Ni nanoparticles are coated on the WC/C framework in clusters. Therefore, these nanocluster nickel dots offer plenty of "active sites" to adsorb the urea molecule, which is advantageous to the electrocatalysis process [38]. Additionally, there are also tungsten carbide particles on the surface working together with nickel. When tungsten carbide is doped into nickel particles, more lattice imperfection would be created thus resulting in more active sites.

The TEM images of the Ni–WC/C catalyst are shown in Fig. 4. From Fig. 4a, it is interesting to note that numerous small dark spots are uniformly dispersed on the substrate, which is similar to the SEM images. The high-resolution TEM image (see Fig. 4b) taken from the edge of a grape-like sphere further demonstrates that the nanoscale nickel is loaded onto the WC/C framework. The nanocrystals with lattice spacing of ca. 0.20 nm and ca. 0.25 nm correspond to the (111) planes ($2\theta = 44.5°$) of nickel [36] and the (100) planes ($2\theta = 35.66°$) of carbide tungsten [37], respectively, which are consistent with the XRD spectrum. The results in Fig. 4 indicate the co-existence of crystalline Ni and WC supported on the activated carbon of the prepared catalyst, which agree well with the SEM images, XRD patterns and EDX data. Accordingly, it can be concluded that the nanoparticles prepared in this work include nickel and tungsten carbide nanocrystals.

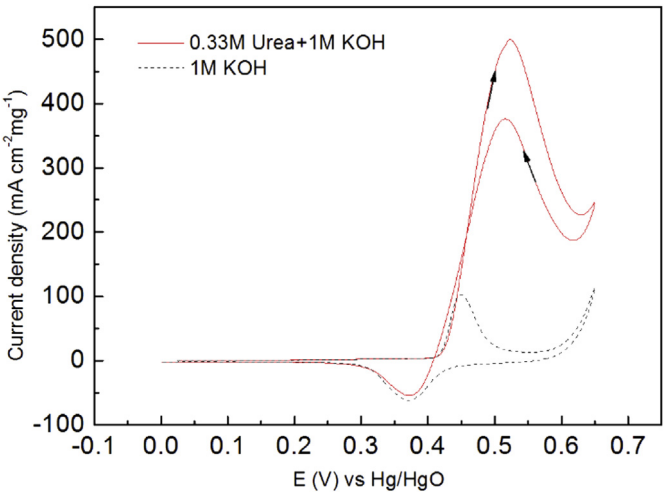


**Fig. 5.** Cyclic voltammograms of the 10% Ni–10% WC/C catalyst (sample A) in 1 M KOH solution in the absence and presence of 0.33 M urea at a scan of 10 mV $s^{-1}$.

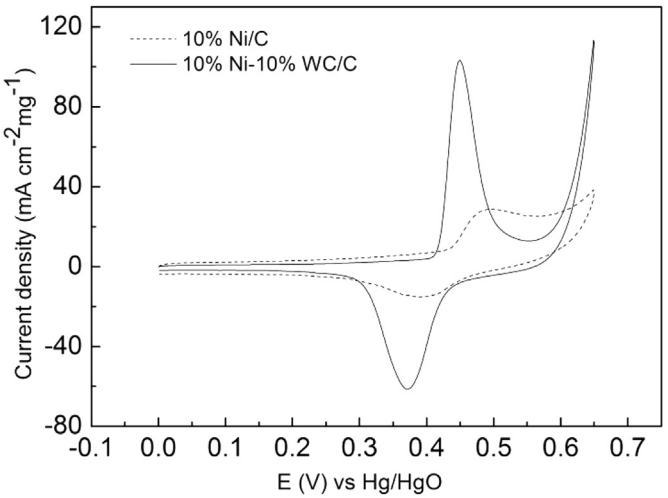


**Fig. 7.** Comparison of 10% Ni/C and 10% Ni–10% WC/C electrodes in 1 M KOH alone at a scan of 10 mV $s^{-1}$.

### 3.2. Electrocatalytic activity of Ni–WC/C catalysts for the urea electrooxidation

The electrochemical behavior of the 10% Ni–10% WC/C (sample A) modified electrode for urea electrooxidation was investigated by cyclic voltammetry (CV). Fig. 5 shows the CVs of the sample A in 1 M KOH solution in the absence and presence of 0.33 M urea. Without addition of urea, the dashed curve reveals a relatively low peak at 0.45 V in 1 M KOH (baseline), which is related to the oxidation–reduction reaction of $Ni(OH)_2$ and NiOOH in alkaline media [3]. In the presence of urea, the curve shows a significantly higher oxidation peak than that in background KOH, which confirms the electrooxidation of urea [5]. The drastic increase of oxidation current commencing at 0.42 V where NiOOH is generated indicates that NiOOH is the active form for urea electrooxidation [5,11,12]. The results demonstrate that the Ni–WC/C catalyst yields high electrocatalytic activity towards urea electrooxidation, and the main active form is NiOOH in alkaline media which has also been observed for other Ni based catalysts [3,4,8,11,13].

For comparison, the electrocatalytic activities of 10% Ni/C and 10% WC/C for urea electrooxidation were investigated by CVs in 1 M KOH solution in the presence of 0.33 M urea, as shown in Fig. 6. The figure shows that Ni/C can also catalyze urea electrooxidation whereas there is no clear oxidation peaks for the WC/C electrode in the solution. However, the urea electrooxidation current density catalyzed by Ni–WC/C is much higher than that of the Ni/C catalyst. This suggests a synergistic catalysis between Ni and WC because the Ni–WC/C catalyst provides higher current density than either Ni/C or WC/C alone. It turns out that the catalytic activity for urea electrooxidation is significantly enhanced by the addition of WC.

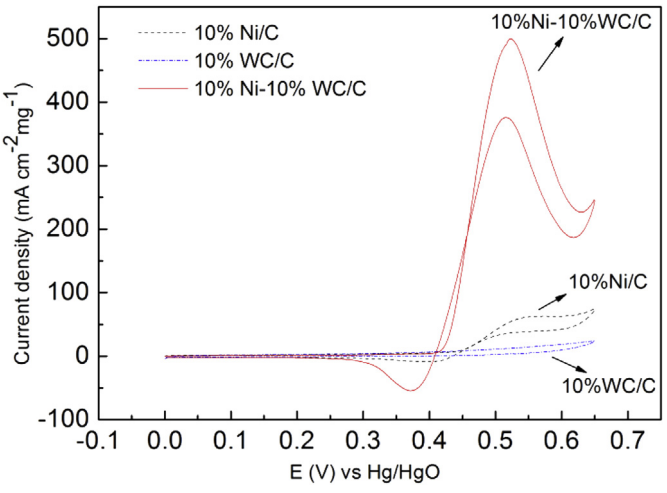


**Fig. 6.** Comparison of 10% Ni/C, 10% WC/C and 10% Ni–10% WC/C electrodes for the urea electrooxidation in 1 M KOH + 0.33 M urea at a scan of 10 mV $s^{-1}$.

### 3.3. Analysis of urea electrooxidation enhancement by Ni–WC/C nanoclusters catalyst

To evaluate the effect of WC in the Ni–WC/C catalyst, CV sweeps of 10% Ni/C and 10% Ni–10% WC/C electrodes in 1 M KOH solution in the absence of urea were performed, shown as curves in Fig. 7. The peaks in each CV are the formation of NiOOH on the forward scan and $Ni(OH)_2$ on the reverse scan, as expected (Eq. (2)). It is notable in Fig. 7 that the real electrochemical-active area of Ni–WC/C is larger than that of Ni/C, indicating that the particle size of Ni on Ni–WC/C is much smaller than that of Ni/C. The electrochemical surface area (ESA) of the Ni catalyst on the electrode surface has been estimated using the charge required to reduce NiOOH to $Ni(OH)_2$ during the cathodic sweeps according to the reported literature. [13] The calculated results (in Table 2) reveal that the Ni–WC/C is provided with a larger ESA (50.73 $m^2\ g^{-1}$) than that of the Ni/C (14.67 $m^2\ g^{-1}$). The Ni–WC/C catalyst with larger ESA offers more active sites, which may be attributed to the structure effect due to the doping of WC to Ni. Furthermore, the results in Table 2 indicate that the Ni–WC/C also exhibits a higher specific activity (3.4 A $m^{-2}$ Ni) which is 1.17 times the specific activity of the Ni/C (2.9 A $m^{-2}$

**Table 2**
Electrochemical activities of the formation of NiOOH for Ni/C and Ni–WC/C.

| Catalyst | ESA[a] ($m^2\ g^{-1}$) | Mass activities (mA $mg^{-1}$ Ni) | Specific activities (A $m^{-2}$ Ni) |
|---|---|---|---|
| Ni/C | 14.67 | 42.9 | 2.9 |
| Ni–WC/C | 50.73 | 173.4 | 3.4 |

[a] The value of ESA is calculated according to the following formula: ESA = $Q$/0.257*$m$. The $Q$ (mC) consumed during the reduction of NiOOH to $Ni(OH)_2$ has been estimated by integration of the area under the reduction peak of the CVs shown in Fig. 7. A 0.257 mC $cm^{-2}$ is the charge associated with the formation of a monolayer of $Ni(OH)_2$, and $m$ is the loading amount of the catalysts.

Ni). Besides, the onset potential of the Ni–WC/C catalyst is 40 mV more negative than that of the Ni/C catalyst, indicating that the active NiOOH is easily formed on the Ni–WC/C catalyst. The higher specific activity and lower onset potential of the Ni–WC/C catalyst could be ascribed to the synergistic effect between Ni and WC. It indicates that both the structure effect and the electron effect accelerate the formation of more active NiOOH for urea electrooxidation.

To further clarify the electronic effect of WC on Ni, XPS measurements were performed. The XPS spectra for Ni 2p of Ni/C and Ni–WC/C are shown in Fig. 8 and reference data are presented in Table 3. The characteristic Ni 2p peaks which are associated with the spin-orbit coupling effect require careful analysis because Ni exists in various oxidation states with their overlapping 2p region. For both WC/C and Ni–WC/C, the Ni 2p spectra are well fit by four peaks, and each peak represents to one state of elemental Ni, corresponding to Ni, NiO, $Ni(OH)_2$ and NiOOH. [39] As compared to those of Ni/C, all the peaks of the Ni–WC/C display big positive shifts, especially the peak of NiOOH (from 857.58 to 859.05 eV), which could be attributed to the electron transfer from Ni to WC. Given the big difference in the electro-negativity between Ni and WC, the shifts of d electron density from Ni to WC would lower the outer-layer electron density of Ni, thus weakening the penetration effect of outer-layer electron to the more inner layer. Hence, the decreased outer-layer electrons reduce shielding effect for the

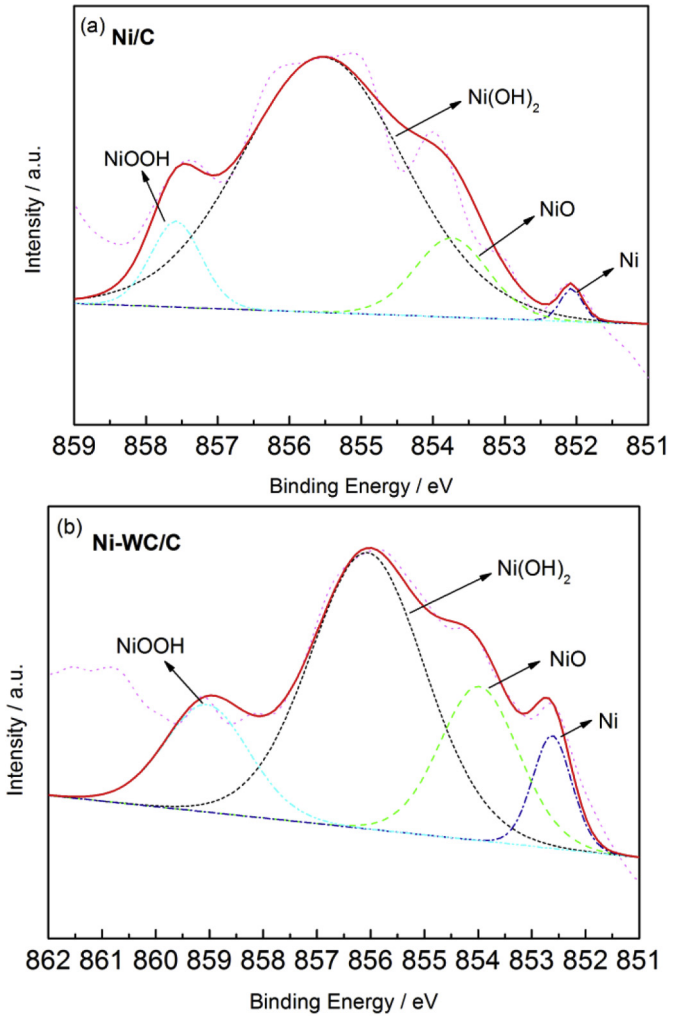


**Fig. 8.** XPS spectra of Ni 2p from the (a) Ni/C and (b) Ni–WC/C catalysts.

**Table 3**
XPS reference data for Ni 2p of the Ni/C and Ni–WC/C catalysts.

| | Ni/C | | Ni–WC/C | |
|---|---|---|---|---|
| | BE (eV) | Compositions (%) | BE (eV) | Compositions (%) |
| Ni | 852.07 | 1.40 | 852.62 | 7.67 |
| NiO | 853.74 | 11.07 | 853.98 | 21.16 |
| $Ni(OH)_2$ | 855.53 | 79.21 | 856.06 | 55.29 |
| NiOOH | 857.58 | 8.31 | 859.05 | 15.88 |

constraining force of nuclear charge and enhance the attraction of atomic nucleus to 2p electrons. [40] Thus, Ni 2p electrons are inspired difficultly and their binding energy would be a positive shift.

Quantitative XPS results of both Ni/C and Ni–WC/C, shown in Table 3, indicate the percentages of surface Ni in each state and their binding energy positions. Compared with the percentage of NiOOH in both samples, it is also observed that the percentage of surface NiOOH increased from 8.31% to 15.88% with the presence of WC, indicating that more NiOOH tends to be generated on the surface of the Ni–WC/C catalyst. It is inferred that doping tungsten carbide to nickel leads to the electronic distribution of the new catalyst in a desirable direction [29,41], resulting in more "active state". Herein, it is concluded that the more active state (NiOOH) for urea electrooxidation is formed which enhances the catalytic activity.

### 3.4. Optimum composition of Ni–WC/C catalysts for the urea electrooxidation

In order to optimize the composition, different contents of Ni–WC/C catalysts (samples A–E) were investigated by a group of cyclic voltammograms (CVs) in 1 M KOH + 0.33 M urea. It can be seen that all of the Ni–WC/C catalysts with different contents provide higher current densities than the Ni/C catalyst, as shown in Fig. 9. Additionally, it is shown that the 20% Ni–20% WC/C (sample D) electrode offers the highest current density for urea electrooxidation. The maximum peak current density is 682.94 mA $cm^{-2}$ $mg^{-1}$, which is about one order of magnitude higher than that offered by the Ni/C; furthermore, it shows ca. 100 times enhancement in current density compared with other reported studies for urea electrooxidation [1,13]. Therefore, the 20%

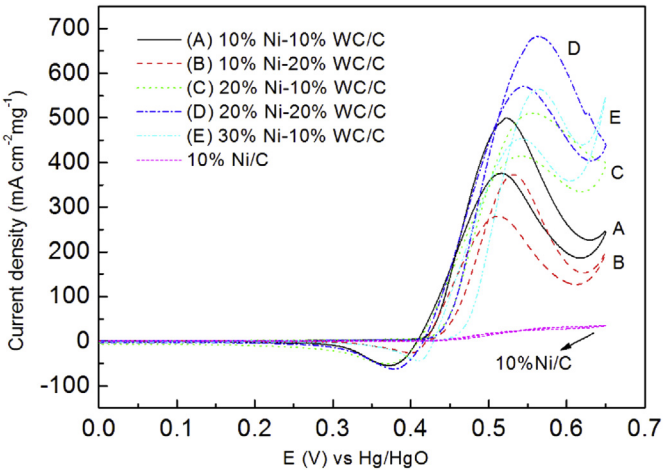


**Fig. 9.** CVs of different contents of Ni–WC/C catalysts (samples A–E) and comparison of Ni/C catalyst used for the urea electrooxidation. Cyclic voltammetry of each catalyst was performed from 0 to 0.65 V vs. Hg/HgO at 10 mV $s^{-1}$ in 1 M KOH + 0.33 M urea.

Ni–20% WC/C (sample D) catalyst appears to be the optimum content for urea electrooxidation under our experimental condition. It is hypothesized that this particular content provides sufficient nickel on the surface for the catalytic process because nickel is the main catalyst for urea electrooxidation but excess nickel would hinder the effect of tungsten carbide. Consequently, the 20% Ni–20% WC/C (sample D) catalyst displaying the highest catalytic activity for urea electrooxidation is regarded as the optimum content.

### 3.5. Electrocatalytic stability of Ni–WC/C catalysts for the urea electrooxidation

The electro-catalytic stabilities of the Ni–WC/C catalysts (samples A–E) were evaluated by the chronoamperometry at 0.50 V in 1 M KOH solution in the presence of 0.33 M urea, as shown in Fig. 10. From this figure, the steady current density catalyzed by each Ni–WC/C sample is much higher than that by the Ni/C catalyst for urea electrooxidation. Nevertheless, the Ni/C electrode nearly lost its catalytic activity during the long-time test. It also can be seen that the sample D (20% Ni–20% WC/C) demonstrated the highest steady current density for the urea electrooxidation, which is in accordance with the CV features. The highest steady current density remains at 92.59 mA $cm^{-2}$ $mg^{-1}$ after 3600 s at the Ni–WC/C electrode, indicating the superior stability for the urea electrooxidation.

The incorporation of tungsten carbide results in stability improvement, which may be attributed to its high CO-resistance. The theoretical investigation of Daramola et al. [11] shows that CO groups tend to strongly adsorb on the surface of the NiOOH which may quickly lose its catalytic activity during the urea electrooxidation. However, the adsorption of CO on WC is very weak. The addition of WC on the surface would impede CO adsorption on the active sites, and hence allowing the active sites (NiOOH) to perform their duty. Thus, the catalytic stability for urea electrooxidation is greatly improved by the addition of WC in the Ni-based catalyst. Given the advantages of higher electrooxidation activity, CO-resistance and stability for the Ni–WC/C case, this kind of catalyst holds significant potential for practical applications in urea electrooxidation.

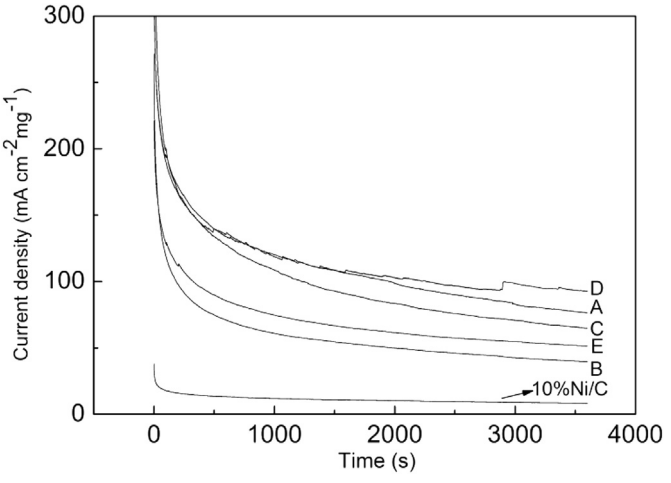


**Fig. 10.** Chronoamperograms of different contents of Ni–WC/C catalysts (samples A–E) and 10% Ni/C in 1 M KOH solution in the presence of 0.33 M urea. (A) 10% Ni–10% WC/C, (B) 10% Ni–20% WC/C, (C) 20% Ni–10% WC/C, (D) 20% Ni–20% WC/C, (E) 30% Ni–10% WC/C. Applied potential was 0.5 V vs. Hg/HgO.

## 4. Conclusions

In the present work, a Ni–WC/C catalyst was prepared by a sequential impregnation method for the first time. The Ni nanoparticles are in clusters which are uniformly distributed on the WC/C framework. The Ni–WC/C nanocluster catalyst shows high electrocatalytic activity and stability for urea electrooxidation. The maximum current density of urea electrooxidation exhibited by the Ni–WC/C catalyst is almost 700 mA $cm^{-2}$ $mg^{-1}$, which is one order of magnitude higher than that of displayed by the Ni/C electrode. Furthermore, the ESA of the Ni–WC/C catalyst (50.73 $m^2$ $g^{-1}$) is larger than that of the Ni/C catalyst (14.67 $m^2$ $g^{-1}$), indicating that the particle size of Ni on the former is much smaller than that of the latter. The Ni 2p peaks in the XPS spectra of the Ni–WC/C catalyst show big positive shifts compared to those of Ni/C, especially the peak of NiOOH (1.47 eV shift), which are attributed to the electron transfer from Ni to WC. Therefore, the addition of tungsten carbide contributes to the formation of the active form NiOOH for urea electrooxidation. Additionally, the longer current-time test reveals that the stable current density of the Ni–WC/C catalyst is also superior to that of the Ni/C catalyst.

The Ni–WC/C nanocluster catalyst described here is able to simultaneously exhibit three key characteristics of a good, practical catalyst for urea electrooxidation: high electro-activity, great tolerance to poisoning, and high stability. The enhanced performance of the Ni–WC/C catalyst for urea electrooxidation could be attributed to the synergistic effect between nickel and tungsten carbide, as well as to its nanocluster structure. The mechanism by which this novel catalyst enhances the extent of urea electrooxidation could be further investigated by Density Functional Theory (DFT) calculations. Our laboratory will explore this subject area and the results will be reported in future communications.

## Acknowledgment

Financial support for this work from the National Natural Science Foundation of China (No. 21276203 and No. 21303132) and Specialized Research Fund for the Doctoral Program of Higher Education of China (No. 20110201130002) are gratefully acknowledged.

## References

[1] R. Ji, D. Chan, J. Jow, M. Wu, Electrochem. Commun. 29 (2013) 21–24.
[2] A.N. Rollinson, J. Jones, V. Dupont, M.V. Twigg, Energy Environ. Sci. 4 (2011) 1216–1224.
[3] B.K. Boggs, R.L. King, G.G. Botte, Chem. Commun. (2009) 4859–4861.
[4] W. Yan, D. Wang, G.G. Botte, Electrochim. Acta 61 (2012) 25–30.
[5] R.L. King, G.G. Botte, J. Power Sources 196 (2011) 2773–2778.
[6] W. Yan, D. Wang, G.G. Botte, Appl. Catal. B Environ. 127 (2012) 221–226.
[7] A.T. Miller, B.L. Hassler, G.G. Botte, J. Appl. Electrochem. 42 (2012) 925–934.
[8] R.L. King, G.G. Botte, J. Power Sources 196 (2011) 9579–9584.
[9] R. Lan, S.W. Tao, J. Irvine, Energy Environ. Sci. 3 (2010) 438–441.
[10] S.J. Ewing, R. Lan, X.X. Xu, S.W. Tao, Fuel Cells 10 (2010) 72–76.
[11] D.A. Daramola, D. Singh, G.G. Botte, J. Phys. Chem. A 114 (2010) 11513–11521.
[12] V. Vedharathinam, G.G. Botte, Electrochim. Acta 81 (2012) 292–300.
[13] D. Wang, W. Yan, S.H. Vijapur, G.G. Botte, J. Power Sources 217 (2012) 498–502.
[14] D. Wang, W. Yan, G.G. Botte, Electrochem. Commun. 13 (2011) 1135–1138.
[15] E. Proietti, F. Jaouen, M. Lefevre, N. Larouche, J. Tian, J. Herranz, J.P. Dodelet, Nat. Commun. 2 (2011).
[16] R. Lan, J.T.S. Irvine, S. Tao, Int. J. Hydrogen Energy 37 (2012) 1482–1494.
[17] Y. Wang, S. Song, V. Maragou, P.K. Shen, P. Tsiakaras, Appl. Catal. B Environ. 89 (2009) 223–228.
[18] D.V. Esposito, S.T. Hunt, Y.C. Kimmel, J. Chen, J. Am. Chem. Soc. 134 (2012) 3025–3033.
[19] H.J. Zheng, J.G. Huang, W. Wang, C.N. Ma, Electrochem. Commun. 7 (2005) 1045–1049.
[20] G.H. Li, C.A. Ma, Y.F. Zheng, W.M. Zhang, Microporous Mesoporous Mater. 85 (2005) 234–240.
[21] F.P. Hu, G.F. Cui, Z.D. Wei, P.K. Shen, Electrochem. Commun. 10 (2008) 1303–1306.
[22] M.B. Zellner, J.G. Chen, Catal. Today 99 (2005) 299–307.

[23] R. Ganesan, J.S. Lee, Angew. Chem. Int. Ed. 44 (2005) 6557–6560.
[24] R. Ganesan, D.J. Ham, J.S. Lee, Electrochem. Commun. 9 (2007) 2576–2579.
[25] D.J. Ham, Y.K. Kim, S.H. Han, J.S. Lee, Catal. Today 132 (2008) 117–122.
[26] D.R. McIntyre, G.T. Burstein, A. Vossen, J. Power Sources 107 (2002) 67–73.
[27] W.T. Yu, Z.J. Mellinger, M.A. Barteau, J. Chen, J. Phys. Chem. C 116 (2012) 5720–5729.
[28] H. Kim, I. Shon, J. Yoon, J. Doh, Z.A. Munir, Int. J. Refract. Met. Hard Mater. 24 (2006) 427–431.
[29] R.B. Levy, M. Boudart, Science 181 (1973) 547–549.
[30] L.H. Bennett, J.R. Cuthill, A.J. McAlister, N.E. Erickson, Science 187 (1975) 858–859.
[31] A. Lofberg, L. Seyfried, P. Blehen, S. Decker, J.M. Bastin, A. Frennet, Catal. Lett. 33 (1995) 165–173.
[32] M.H. Shao, B. Merzougui, K. Shoemaker, L. Stolar, L. Protsailo, Z.J. Mellinger, I.J. Hsu, J. Chen, J. Power Sources 196 (2011) 7426–7434.
[33] J. Sun, M.Y. Zheng, X.D. Wang, A.Q. Wang, R. Cheng, T. Li, T. Zhang, Catal. Lett. 123 (2008) 150–155.
[34] Y. Hara, N. Minami, H. Matsumoto, H. Itagaki, Appl. Catal. A Gen. 332 (2007) 289–296.
[35] X. Yang, Y. Liu, S. Li, X. Wei, L. Wang, Y. Chen, Sci. Rep. 2 (2012) 567.
[36] S. Wu, D. Chen, J. Colloid Interface Sci. 259 (2003) 282–286.
[37] M. Nie, H.L. Tang, Z.D. Wei, S.P. Jiang, P.K. Shen, Electrochem. Commun. 9 (2007) 2375–2379.
[38] G.L. Che, B.B. Lakshmi, C.R. Martin, E.R. Fisher, Langmuir 15 (1999) 750–758.
[39] Z.B. Wang, P.J. Zuo, G.J. Wang, C.Y. Du, G.P. Yin, J. Phys. Chem. C 112 (2008) 6582–6587.
[40] J. Yang, Y. Xie, R. Wang, B. Jiang, C. Tian, G. Mu, J. Yin, B. Wang, H. Fu, ACS Appl. Mater. Interfaces 5 (2013) 6571–6579.
[41] L.H. Bennett, J.R. Cuthill, A.J. McAlister, N.E. Erickson, R.E. Watson, Science 184 (1974) 563–565.